Orientation relationship of intergrowth Al_2Fe and Al_5Fe_2 intermetallics determined by single crystal X-ray diffraction

Yibo Liu [1], Changzeng Fan [1,2]*, Bin Wen [1], Zhefeng Xu [1,2], Ruidong Fu [1,2], Lifeng Zhang [1,3].

[1] State Key Laboratory of Metastable Materials Science and Technology, Yanshan University, Qinhuangdao 066004, People's Republic of China

[2] Hebei Key Lab for Optimizing Metal Product Technology and Performance, Yanshan University, Qinhuangdao 066004, People's Republic of China.

[3] School of Mechanical and Materials Engineering, North China University of Technology, Beijing 100144, People's Republic of China

* Correspondence: chzfan@ysu.edu.cn

Supplementary materials include:

Figure S1 (a) The Phi360 diffraction pattern collected in the process of single crystal testing, (b) the powder diffraction pattern obtained by integrating the Phi360 diffraction pattern.

Table S1 EDX component analysis at each scanning spot

Figure S2 Scanning Electron Microscope (SEM) micrographs of single crystal sample. EDX analysis were performed on different sites corresponding to those listed in Table S1

Table S2 EDX component analysis at each scanning spot and area

Figure S3 Scanning Electron Microscope (SEM) micrographs of single crystal sample. EDX analysis were performed on different sites corresponding to those listed in Table S2

Figure S4 Structural relationships between the parent η-Fe_2Al_5, Al-rich low-temperature η′-Fe_3Al_8, and Fe-rich low temperature η″-Fe_3Al_{7+x} phases

Figure S5 The precession images of intergrowth crystals: (a) $Al_{12.48}Fe_{6.52}(1kl)$, (b) $Al_{12.48}Fe_{6.52}(h1l)$, (c) $Al_{12.48}Fe_{6.52}(hk1)$, (d) $Al_{5.72}Fe_2(1kl)$, (e) $Al_{5.72}Fe_2(h1l)$, (f) $Al_{5.72}Fe_2(hk1)$

Figure S6 The precession images of intergrowth crystals: (a) $Al_{12.48}Fe_{6.52}(2kl)$, (b) $Al_{12.48}Fe_{6.52}(h2l)$, (c) $Al_{12.48}Fe_{6.52}(hk2)$, (d) $Al_{5.72}Fe_2(2kl)$, (e) $Al_{5.72}Fe_2(h2l)$, (f) $Al_{5.72}Fe_2(hk2)$

Figure S7 The precession images of intergrowth crystals: (a) $Al_{12.48}Fe_{6.52}(3kl)$, (b) $Al_{12.48}Fe_{6.52}(h3l)$, (c) $Al_{12.48}Fe_{6.52}(hk3)$, (d) $Al_{5.72}Fe_2(3kl)$, (e) $Al_{5.72}Fe_2(h3l)$, (f) $Al_{5.72}Fe_2(hk3)$

Figure S8 The precession images of intergrowth crystals: (a) $Al_{12.48}Fe_{6.52}(4kl)$, (b) $Al_{12.48}Fe_{6.52}(h4l)$, (c) $Al_{12.48}Fe_{6.52}(hk4)$, (d) $Al_{5.72}Fe_2(4kl)$, (e) $Al_{5.72}Fe_2(h4l)$, (f) $Al_{5.72}Fe_2(hk4)$

Figure S9 The precession images of intergrowth crystals: (a) $Al_{12.48}Fe_{6.52}(5kl)$, (b) $Al_{12.48}Fe_{6.52}(h5l)$, (c) $Al_{12.48}Fe_{6.52}(hk5)$, (d) $Al_{5.72}Fe_2(5kl)$, (e) $Al_{5.72}Fe_2(h5l)$, (f) $Al5_{.72}Fe_2(hk5)$

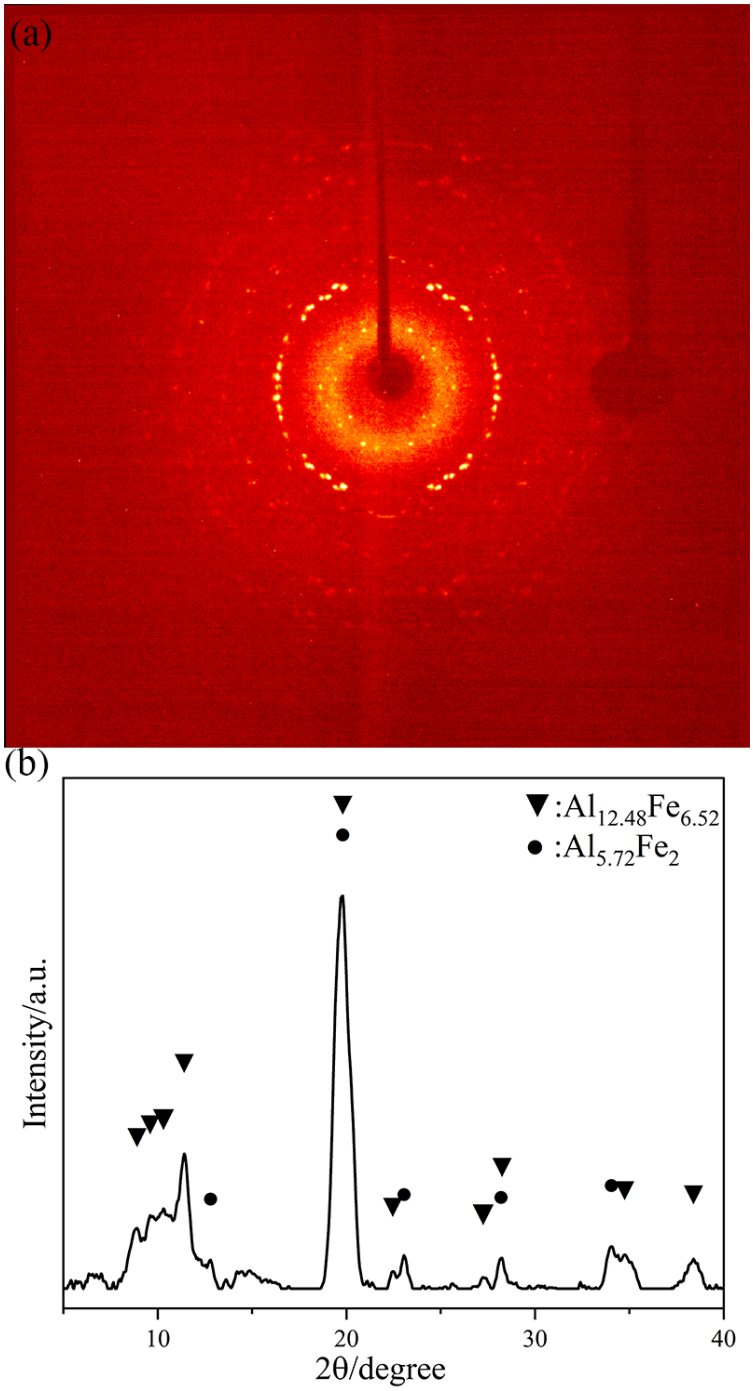

Figure S1 (a) The Phi360 diffraction pattern collected in the process of single crystal testing, (b) the powder diffraction pattern obtained by integrating the Phi360 diffraction pattern.

It can be seen from Figure S1 that the $Al_{12.48}Fe_{6.52}$ and $Al_{5.72}Fe_2$ phases are the dominant phases and there are also few weak peaks which do not belong to phases that may attribute to tiny crystalline phases or amorphous phase.

In order to determine the single crystal morphology and the proportion of elements in the target sample obtained by sintering, Hitachi S-3400 field emission scanning electron microscope (SEM) was used to observe the morphology of single crystal samples, the elements

in the samples were analyzed by energy dispersive X-ray spectroscopy (EDX), which was used in electron microscopy, the types and corresponding contents of the elements were analyzed. Concerning the selected fragment of the single crystal sample, EDX analysis was carried out on six spots (see Figure S2) and the corresponding results are listed in Table S1. It can be seen that the atomic ratio of Al-Fe at Spot1 and Spot2 is quite different from other spots. This also proves that the single crystal is grown from two different single crystals.

Table S1 EDX component analysis at each scanning spot.

	Element	Weight(%)	Atomic(%)	Error(%)	Al:Fe
Spot1	Al	51.64	68.85	6.00	2.21:1
	Fe	48.36	31.15	2.06	
Spot2	Al	53.17	70.15	5.91	2.35:1
	Fe	46.83	29.85	2.14	
Spot3	Al	47.51	65.20	6.26	1.87:1
	Fe	52.49	34.80	2.02	
Spot4	Al	44.60	62.50	6.42	1.67:1
	Fe	55.40	37.50	1.99	
Spot5	Al	47.90	65.55	6.24	1.90:1
	Fe	52.10	34.45	2.05	
Spot6	Al	47.83	65.49	6.24	1.90:1
	Fe	52.17	34.51	2.05	

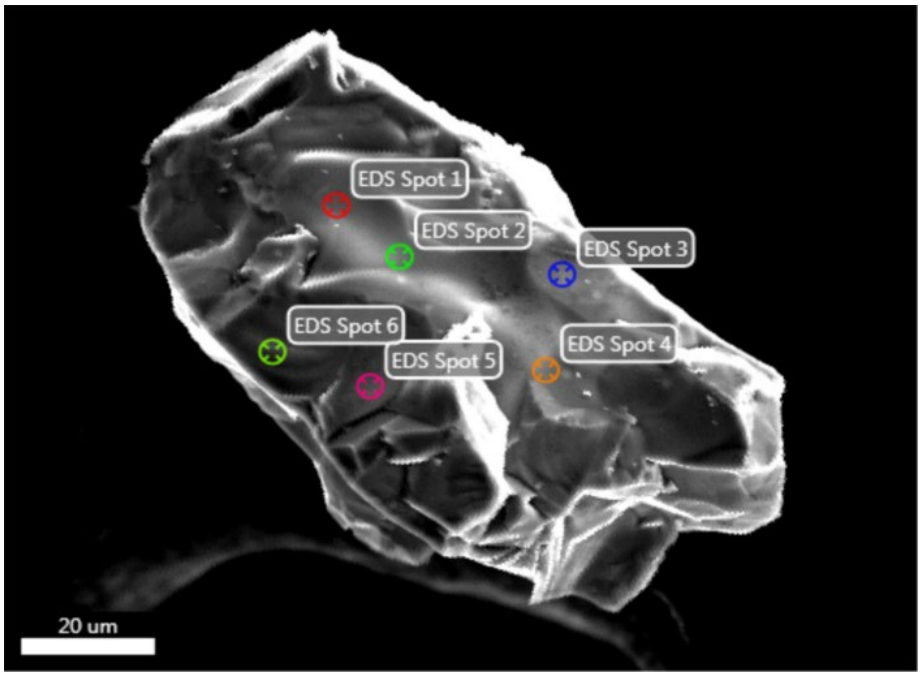

Figure S2 Scanning Electron Microscope (SEM) micrographs of single crystal sample. EDX analysis were performed on different sites corresponding to those listed in Table S1.

The chemical compositions were also examined quantitatively by Oxford spectroscopy (EDX) analysis attached to a ZEISS Sigma 300 field emission SEM for the purpose of guiding

the crystal structure refinement for the same sample from a different perspective. The examined points and areas are designated in Fig. S3, and the corresponding results are listed in Table S2. The deviation relative to the results of refinement of chemical composition is probably caused by the tilt of the single crystal surface to the incident beam. For ease of reading, the atomic ratio of Al, Fe was calculated and shown in the last column of Table S2. In Table S2, the chemical compositions of areas 3 and 5 are in good agreement with $Al_{12.48}Fe_{6.52}$ phase, while those of areas 4 and 6 are in good agreement with $Al_{5.72}Fe_2$ phase.

Table S2 EDX component analysis at each scanning spot and area

	Element	Atomic(%)	Al:Fe
Spot1	Al	76.2	3.20:1
	Fe	23.8	
Area1	Al	71.3	2.48:1
	Fe	28.7	
Area2	Al	76.2	3.20:1
	Fe	23.8	
Area3	Al	68.4	2.16:1
	Fe	31.6	
Area4	Al	74.7	2.95:1
	Fe	25.3	
Area5	Al	65.2	1.87:1
	Fe	34.8	
Area6	Al	73.0	2.70:1
	Fe	27.0	
Area7	Al	70.1	2.34:1
	Fe	29.9	

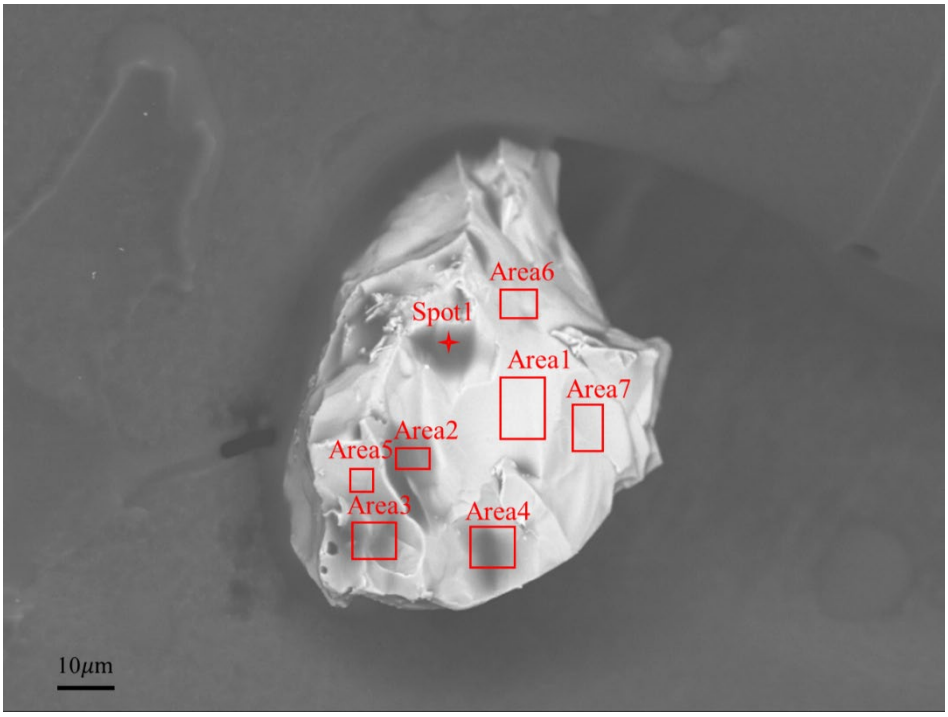

Figure S3 Scanning Electron Microscope (SEM) micrographs of single crystal sample. EDX analysis were performed on different sites corresponding to those listed in Table S1

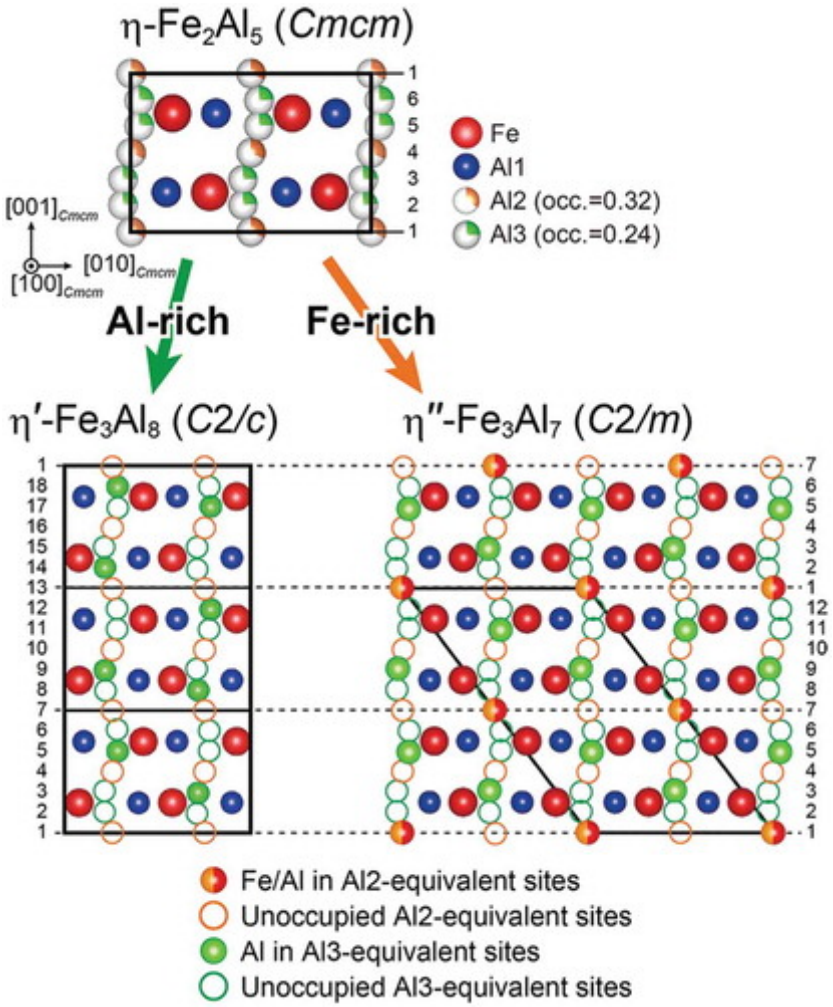

Figure S4 Structural relationships between the parent η-Fe_2Al_5, Al-rich low-temperature η′-Fe_3Al_8, and Fe-rich low temperature η″-Fe_3Al_{7+x} phases (copy from Figure 10 of Reference 14).

As shown in Figure S4, the crystal structure of low temperature phase Al_8Fe_3 and Al_7Fe_3 is constructed based on the crystal structure of $Al_{5.6}Fe_2$ phase. Due to the difference in the occupancy of vacant Al atoms in the $Al_{5.72}Fe_2$ phase and the $Al_{5.6}Fe_2$ phase, we believe that this may lead to the emergence of some modified Al_8Fe_3 and Al_7Fe_3 phases.

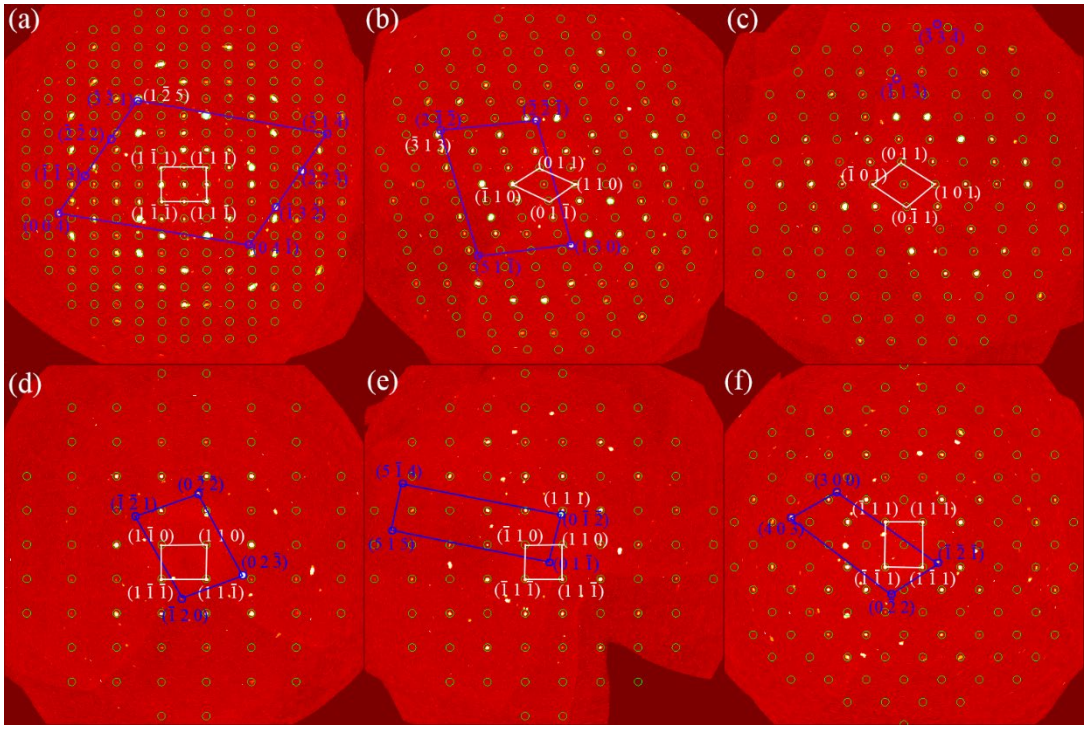

Figure S5 The precession images of intergrowth crystals: (a) $Al_{12.48}Fe_{6.52}(1kl)$, (b) $Al_{12.48}Fe_{6.52}(h1l)$, (c) $Al_{12.48}Fe_{6.52}(hk1)$, (d) $Al_{5.72}Fe_2(1kl)$, (e) $Al_{5.72}Fe_2(h1l)$, (f) $Al_{5.72}Fe_2(hk1)$.

Figure S5 (a), (b) and (c) represent the precession images of the (1*kl*), (*h*1*l*) and (*hk*1) planes from the $Al_{12.48}Fe_{6.52}$ phase while the Figure S5 (d), (e) and (f) represent the precession images of the (1*kl*), (*h*1*l*) and (*hk*1) planes from the $Al_{5.72}Fe_2$ phase. In Figure S5 (a), (b) and (c) the green and blue circle represents the crystal planes of the $Al_{12.48}Fe_{6.52}$ phase and the $Al_{5.72}Fe_2$ phase, respectively, the precession images are constructed with a thickness of 0.05 Å-1 and a resolution of 0.80 Å. While in Figure S5 (d), (e) and (f) the green and blue circle represents the crystal planes of the $Al_{5.72}Fe_2$ phase and the $Al_{12.48}Fe_{6.52}$ phase, respectively, the precession images are constructed with a thickness of 0.03 Å-1 and a resolution of 0.80 Å. Figures S6-S9 use the same Settings as Figure S5. We can find three kinds of crystal plane parallel relationships in Figure S5 (a), (b), (e). They are $(0\bar{2}5)$ $Al_{12.48}Fe_{6.52}$//$(\bar{3}\bar{3}1)$ $Al_{5.72}Fe_2$, $(\bar{3}13)$ $Al_{12.48}Fe_{6.52}$//$(2\bar{4}\bar{2})$ $Al_{5.72}Fe_2$, $(0\bar{1}\bar{2})$ $Al_{12.48}Fe_{6.52}$//(111) $Al_{5.72}Fe_2$.

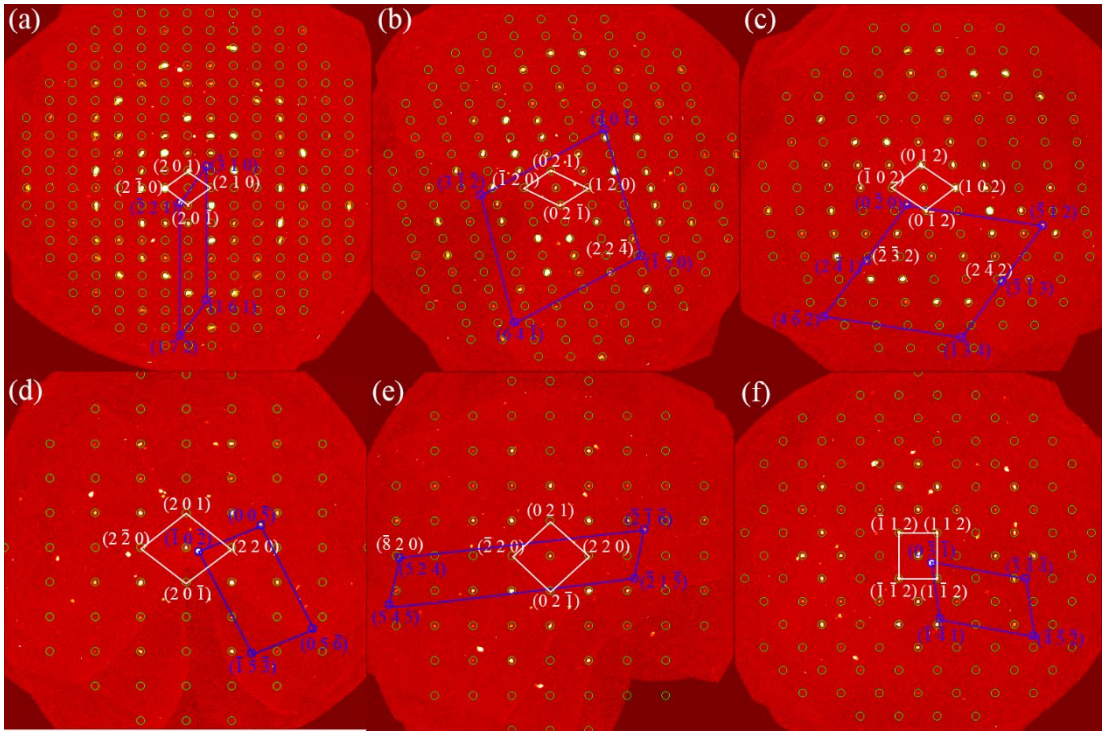

Figure S6 The precession images of intergrowth crystals: (a) $Al_{12.48}Fe_{6.52}(2kl)$, (b) $Al_{12.48}Fe_{6.52}(h2l)$, (c) $Al_{12.48}Fe_{6.52}(hk2)$, (d) $Al_{5.72}Fe_2(2kl)$, (e) $Al_{5.72}Fe_2(h2l)$, (f) $Al_{5.72}Fe_2(hk2)$.

Figure S6 (b), (c), and (d) shows four kinds of crystal plane parallel relationships. They are $(2\bar{2}4)$ $Al_{12.48}Fe_{6.52}$//$(\bar{1}50)$ $Al_{5.72}Fe_2$, $(\bar{2}\bar{3}2)$ $Al_{12.48}Fe_{6.52}$//$(2\bar{4}1)$ $Al_{5.72}Fe_2$, $(2\bar{4}2)$ $Al_{12.48}Fe_{6.52}$//$(\bar{3}\bar{1}3)$ $Al_{5.72}Fe_2$, (524) $Al_{12.48}Fe_{6.52}$//$(\bar{8}20)$ $Al_{5.72}Fe_2$.

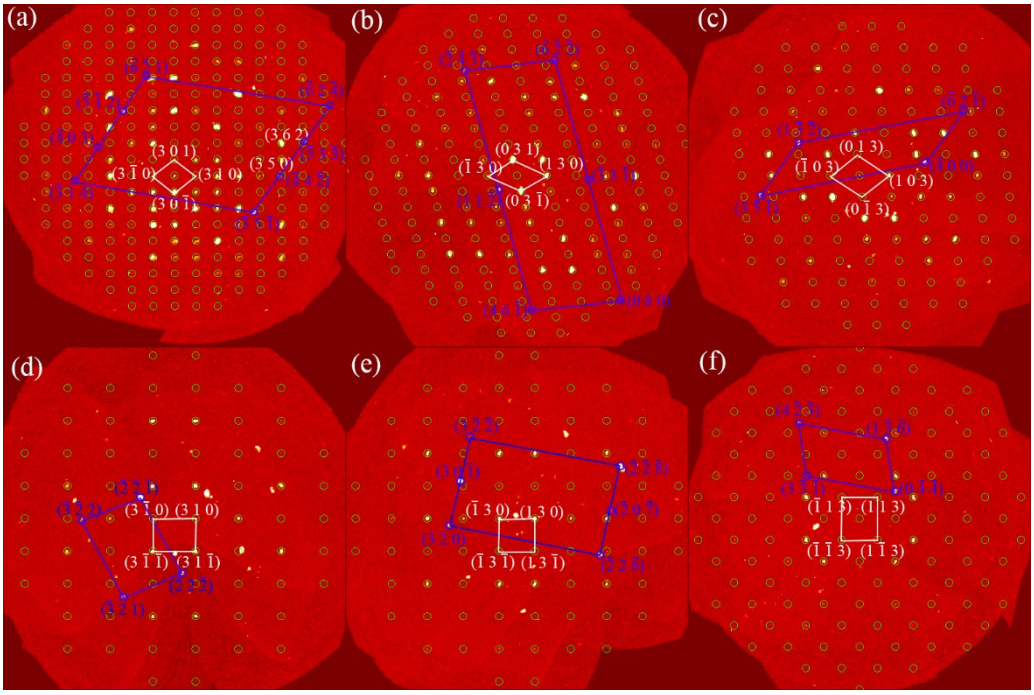

Figure S7 The precession images of intergrowth crystals: (a) $Al_{12.48}Fe_{6.52}(3kl)$, (b) $Al_{12.48}Fe_{6.52}(h3l)$, (c) $Al_{12.48}Fe_{6.52}(hk3)$, (d) $Al_{5.72}Fe_2(3kl)$, (e) $Al_{5.72}Fe_2(h3l)$, (f) $Al_{5.72}Fe_2(hk3)$.

Figure S7 (a) shows two kinds of crystal plane parallel relationships. They are (350) $Al_{12.48}Fe_{6.52}$//($\bar{4}4\bar{2}$) $Al_{5.72}Fe_2$, (362) $Al_{12.48}Fe_{6.52}$//($\bar{5}3\bar{3}$) $Al_{5.72}Fe_2$.

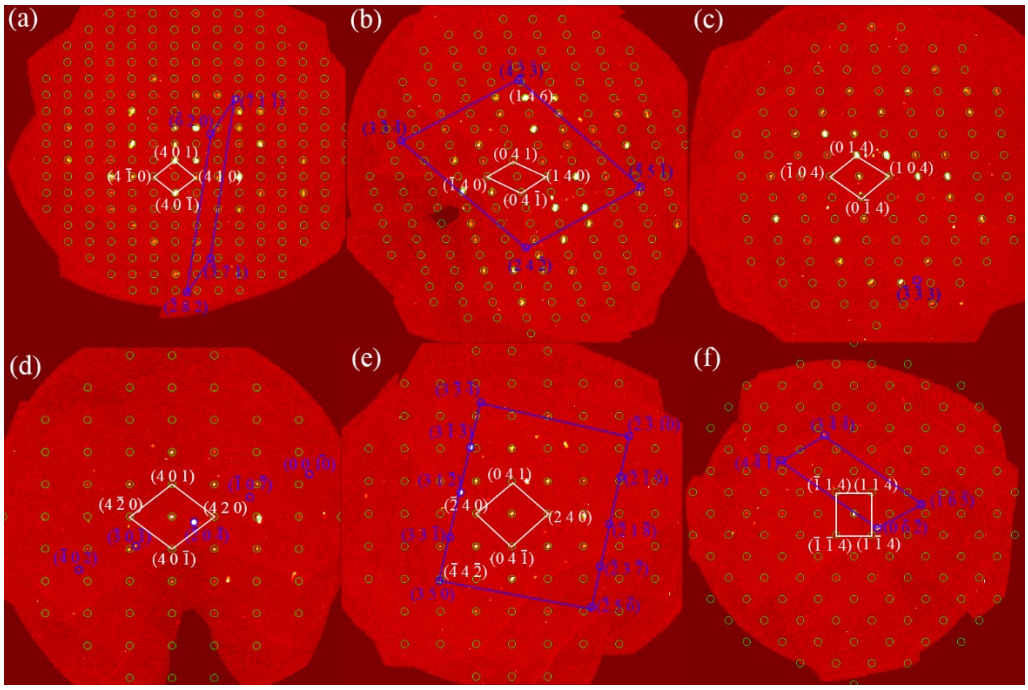

Figure S8 The precession images of intergrowth crystals: (a) $Al_{12.48}Fe_{6.52}(4kl)$, (b) $Al_{12.48}Fe_{6.52}(h4l)$, (c) $Al_{12.48}Fe_{6.52}(hk4)$, (d) $Al_{5.72}Fe_2(4kl)$, (e) $Al_{5.72}Fe_2(h4l)$, (f) $Al_{5.72}Fe_2(hk4)$.

Figure S8 (b), (e) shows two kinds of crystal plane parallel relationships. They are (146) $Al_{12.48}Fe_{6.52}$//($\bar{4}\bar{2}\bar{3}$) $Al_{5.72}Fe_2$, (31$\bar{2}$) $Al_{12.48}Fe_{6.52}$//($\bar{2}40$) $Al_{5.72}Fe_2$.

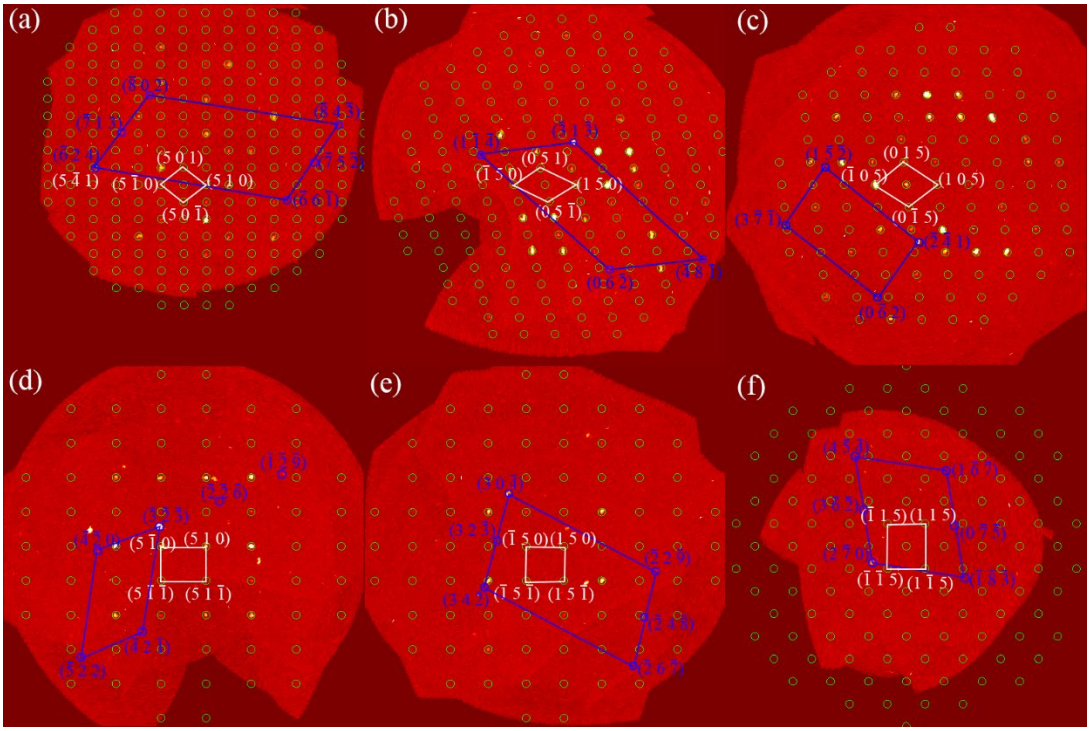

Figure S9 The precession images of intergrowth crystals: (a) $Al_{12.48}Fe_{6.52}(5kl)$, (b)

$Al_{12.48}Fe_{6.52}$(*h*5*l*), (c) $Al_{12.48}Fe_{6.52}$(*hk*5), (d) $Al_{5.72}Fe_2$(5*kl*), (e) $Al_{5.72}Fe_2$(*h*5*l*), (f) $Al_{5.72}Fe_2$(*hk*5).

Figure S9 (a) shows one kind of crystal plane parallel relationship. It is (5 $\bar{4}$ 1) $Al_{12.48}Fe_{6.52}$//($\bar{6}$24) $Al_{5.72}Fe_2$.